Journal of Sound and Vibration 329 (2010) 150–170

Contents lists available at ScienceDirect

Journal of Sound and Vibration

journal homepage: www.elsevier.com/locate/jsvi

Tracking noisy limit cycle oscillation with nonlinear filters

Mohammad Khalil [a], Abhijit Sarkar [a,*], Sondipon Adhikari [b]

[a] Carleton University, Department of Civil and Environmental Engineering, Mackenzie Building, Colonel By Drive, Ottawa, Ontario K1S 5B6, Canada
[b] Swansea University, School of Engineering, Singleton Park, Swansea SA2 8PP, UK

ARTICLE INFO

Article history:
Received 7 December 2007
Received in revised form
4 September 2009
Accepted 9 September 2009
Handling Editor: C.L. Morfey
Available online 9 October 2009

ABSTRACT

For engineering systems, the dynamic state estimates provide valuable information for the detection and prediction of failure due to noise and vibration. From this perspective, nonlinear filtering techniques are applied to the problem of state estimation of dynamical systems undergoing noisy limit cycle oscillation. Specifically, the extended Kalman filter, ensemble Kalman filter and particle filter are used to track the limit cycle oscillations of a Duffing oscillator using noisy observational data. The noisy limit cycle oscillations feature highly non-Gaussian trends. The efficiency and limitations of the extended Kalman filter, ensemble Kalman filter and particle filter in tracking limit cycle oscillations are examined with respect to the model and measurement noise and sparsity of measurement data. For the limit cycle oscillations considered here, it is demonstrated that the ensemble Kalman filter and particle filter outperform the extended Kalman filter in the presence of sparse observational data or strong measurement noise. For moderate measurement noise and frequent measurement data, the ensemble Kalman filter and particle filter perform equally well in comparison to the extended Kalman filter.

1. Introduction

In numerous practical applications in science and engineering, limit cycle oscillation manifests through periodic response of nonlinear dynamical systems (e.g. [1–4]). In engineering systems, limit cycle oscillation is frequently encountered, for example, in vibration of aircraft structures and marine pipelines (e.g. [2,5,6]). The limit cycle oscillation phenomenon is detrimental to the system as it may lead to fatigue or large amplitude response leading to catastrophic failure. Limit cycle oscillation may arise from nonlinearities in the stiffness and damping characteristics of the system and the coupling effect in hydro- and aero-elasticity problems. It is of practical importance to track the state of limit cycle oscillation to assess the safety, reliability and regulatory requirements of the engineering system in its operational state using a set of noisy observational data.

The state estimation problem of dynamical systems has attracted widespread attention, particularly in the data assimilation research community [7–9]. The Kalman filter has become a popular tool for state estimation problems involving linear systems [10,11]. It optimally estimates the state of linear systems in the presence of additive Gaussian model and measurement noise when the observational data is linearly related to the state of the system. The Kalman filter can be extended to weakly nonlinear and non-Gaussian systems by linearizing the model and measurement operators, leading to the popular (but no longer optimal) extended Kalman filter [7,8,12,13]. The major limitation of the Kalman filter and extended Kalman filter stems from the fact that the state evolution is assumed to be Gaussian or approximately Gaussian. Such approximation may lead to poor performance of the extended Kalman filter for strongly nonlinear

* Corresponding author. Tel.: +1 613 520 2600x6320; fax: +1 613 520 3951.
E-mail address: abhijit_sarkar@carleton.ca (A. Sarkar).

0022-460X/$ - see front matter © 2009 Elsevier Ltd. All rights reserved.
doi:10.1016/j.jsv.2009.09.009

dynamical systems [14,15]. To alleviate such problem, the unscented transform [16] is used to propagate the statistical moments of the state vector through the full nonlinear model operator leading to the so-called unscented Kalman filter [17–20]. Using a set of carefully chosen sampling points (so-called sigma points), the unscented Kalman filter estimates the first and second order moments of the state vector correct to the second order Taylor series expansion of the model operator.

A wide range of Monte Carlo based filtering algorithms have been developed to tackle more general classes of nonlinear systems perturbed by non-Gaussian noise. The ensemble Kalman filter is one of the most widely used filtering algorithms based on Monte Carlo sampling technique [7,21–26]. The usefulness of the ensemble Kalman filter has been successfully demonstrated for different applications of data assimilation problems (e.g. [7,23–25]). The ensemble Kalman filter is a computationally efficient technique as it assumes a Gaussian conditional probability density function of the system state based on observational data. In numerous applications, the ensemble Kalman filter resolves the issue of poor error covariance evolution commonly encountered in the extended Kalman filter [27]. In the context of structural dynamics, the ensemble Kalman filter has recently been introduced as a non-parametric identification tool by Ghanem and Ferro [24]. Although widely used, some publications have reported rather poor performance by the ensemble Kalman filter in certain applications in which highly non-Gaussian posterior probability density functions lead to difficulties [25,26]. To alleviate such problems, a non-Gaussian extension of the ensemble Kalman filter has been proposed that utilizes a weighted sum of Gaussian probability density functions (instead of a single Gaussian probability density function) to represent the probability density function of the system state [28,29]. Mandel and Beezley [30] proposed another extension that combines the ensemble Kalman filter with particle filter which involves non-parametric density estimation techniques.

The most general nonlinear filtering algorithm is the so-called particle filter [25,31–39]. This method is formulated in the framework of Bayesian inference and relaxes the assumption of Gaussian conditional probability density functions and linearity of model and measurement operators as assumed in the Kalman filter, extended Kalman filter and ensemble Kalman filter. In the particle filter, the ensemble members (so-called particles) are properly weighted based on the observational data. In general, the particle filter demands larger ensembles compared to the ensemble Kalman filter leading to higher computational efforts, but more effectively tackles strongly non-Gaussian systems. The problem related to the requirement of larger ensembles is partly mitigated using the so-called resampling technique [31,35,36,40]. In the context of nonlinear dynamics, the particle filter was applied to identify a nonlinear stiffness parameter of a Duffing oscillator [36–38]. Kivman [25] compared the applicability of the ensemble Kalman filter and particle filter for parameter estimation in the Lorenz model. Ching et al. [41] compared the performance of the extended Kalman filter and particle filter for the state and parameter estimation of various nonlinear systems. Recently, the authors studied the performance of the extended Kalman filter, ensemble Kalman filter and particle filter for joint state and parameter estimation of a Duffing oscillator undergoing chaotic motion [42]. To improve the performance of the particle filter, hybrid filtering algorithms which combine the extended Kalman filter or unscented Kalman filter with the particle filter have also been proposed leading to the so-called extended Kalman and unscented Kalman particle filters (e.g. [20]).

This investigation compares the feasibility of using the extended Kalman filter, ensemble Kalman filter and particle filter for state estimation of noisy limit cycle oscillations. In particular, period-two subharmonic and period-five subharmonic limit cycle oscillations of a harmonically forced noisy Duffing oscillator are examined. The two limit cycle oscillations demonstrate qualitatively different oscillatory behavior. The Duffing system exhibits a double-well potential and possesses three fixed points, two of which are stable and one is unstable. The stable fixed points identify the location of the potential wells. Despite its mathematical simplicity, the system exhibits a wide range of dynamical response with slight change in input parameters. For the state estimation problem as considered here, the system is perturbed by combined harmonic and random inputs ensuing a transition probability density function of motion which displays strongly non-Gaussian features. An extensive numerical study is undertaken to contrast the performance of aforementioned filtering algorithms with respect to sparsity of observational data and strength of model and measurement noise. A selection of results are presented to bring out the key features of this study.

The paper is organized as follows: A brief background of noisy dynamical systems is presented in Section 2. An overview of the extended Kalman filter is offered in Section 3. the ensemble Kalman filter is briefly introduced in Section 4. In Section 5, the mathematical formulation of the particle filter is reviewed. Section 6 reports the results of numerical investigations which brings out the capabilities and limitations of the filtering algorithms. In Section 7, the paper concludes with a summary of the findings.

2. Background to noisy dynamical systems

The state evolution of a nonlinear dynamical system can be represented by the vector Itô stochastic differential equation [13,43,44]

$$\mathrm{d}\mathbf{x} = \mathbf{m}(\mathbf{x}, t)\,\mathrm{d}t + \mathbf{H}(\mathbf{x}, t)\,\mathrm{d}\mathbf{w}, \tag{1}$$

where $\mathbf{x}$ is an n-dimensional state vector, $\mathbf{m}$ is an n-dimensional random vector function, $\mathbf{H}$ is a $n \times m$ matrix-valued function and $\mathbf{w}$ is an m-dimensional vector Wiener process. The interpretation of the solutions of Eq. (1) is problematical in the classical sense as the solution $\mathbf{x}(t)$ is continuous everywhere but not differentiable anywhere with probability 1 [26].

The transition probability density function $p(\mathbf{x},t|\mathbf{x}_0,t_0)$ of the state vector $\mathbf{x}(t)$ given the initial probability density function of state vector $p(\mathbf{x}_0,t_0)$ is given by Fokker–Planck equation [13,43–45]

$$\frac{\partial p}{\partial t} = -\sum_{i=1}^{n}\frac{\partial}{\partial x_i}\{m_i p\} + \frac{1}{2}\sum_{i,j=1}^{n}\frac{\partial^2}{\partial x_i \partial x_j}\{p(\mathbf{H}\mathbf{H}^{\mathrm{T}})_{ij}\}. \tag{2}$$

For the purpose of tracking the system state, when observational data is available, the transition probability density function is conditioned using Bayes' formula as [13]

$$p(\mathbf{x}_k,t_k|\mathbf{d}_k) = \frac{p(\mathbf{d}_k|\mathbf{x}_k,t_k)p(\mathbf{x}_k,t_k|\mathbf{d}_k^-)}{\int p(\mathbf{d}_k|\mathbf{x}_k,t_k)p(\mathbf{x}_k,t_k|\mathbf{d}_k^-)\,\mathrm{d}\mathbf{x}_k}, \tag{3}$$

where $p(\mathbf{x}_k,t_k|\mathbf{d}_k^-)$ is the probability density function given by the Fokker–Planck equation up to but not including the new observation $\mathbf{d}_k$. $p(\mathbf{d}_k|\mathbf{x}_k,t_k)$ is the probability density function of the observation $\mathbf{d}_k$ given the current state vector $\mathbf{x}_k$. Except for special cases, the exact analytical expression for the conditional probability density function is not available. For practical applications involving general nonlinear systems, one resorts to numerical approximations using nonlinear filters [13,7].

3. Extended Kalman filter

In Ref. [42], we have discussed the extended Kalman filter, ensemble Kalman filter and particle filter in the context of joint state and parameter estimation of a Duffing oscillator undergoing chaotic motion. For the sake of completeness, we briefly review the extended Kalman filter in this Section and the ensemble Kalman filter and particle filter in the following sections. For weakly non-Gaussian systems, the probability density function of the system state $\mathbf{x}$ can be approximated by a Gaussian probability density function through linearization. The discrete state-space representation of a general nonlinear dynamical system with additive model noise and a linear measurement operator is described by

$$\mathbf{x}_{k+1} = \boldsymbol{\Psi}_k(\mathbf{x}_k,\mathbf{f}_k) + \mathbf{q}_k, \tag{4}$$

$$\mathbf{d}_k = \mathbf{C}_k\mathbf{x}_k + \boldsymbol{\varepsilon}_k, \tag{5}$$

where $\mathbf{x}\in\mathbb{R}^n$ is the state vector, $\boldsymbol{\Psi}\in\mathbb{R}^n$ is the discrete nonlinear model operator, $\mathbf{f}\in\mathbb{R}^p$ is a deterministic input, $\mathbf{d}\in\mathbb{R}^m$ is the measurement vector which relates to the true state by the measurement matrix $\mathbf{C}\in\mathbb{R}^{m\times n}$, $\mathbf{q}\in\mathbb{R}^n$ and $\boldsymbol{\varepsilon}\in\mathbb{R}^m$ are independent zero-mean Gaussian vector random processes with covariance matrices $\mathbf{Q}\in\mathbb{R}^{n\times n}$ and $\boldsymbol{\Gamma}\in\mathbb{R}^{m\times m}$, denoting model and measurement errors, respectively. Note that the extended Kalman filter is not restricted to additive model and measurement noise only. For the general case of multiplicative model and measurement noise, the following analysis can be generalized by taking recourse to linearization of the model and measurement operators (e.g. [20]).

It is assumed that $\mathbf{x}$ has a Gaussian prior probability density function given by $\mathbf{x}_k\sim\mathcal{N}(\mathbf{x}_k^f,\mathbf{P}_k)$. The extended Kalman filter then estimates the conditional mean $\mathbf{x}_k^a$ and covariance $\hat{\mathbf{P}}_k$ of $\mathbf{x}_k$ given the measurement vector $\mathbf{d}_k$. This constitutes the analysis step as borrowed from the Kalman filter:

Analysis step:

$$\mathbf{K}_k = \mathbf{P}_k\mathbf{C}_k^{\mathrm{T}}[\boldsymbol{\Gamma}_k + \mathbf{C}_k\mathbf{P}_k\mathbf{C}_k^{\mathrm{T}}]^{-1}, \tag{6}$$

$$\mathbf{x}_k^a = \mathbf{x}_k^f + \mathbf{K}_k(\mathbf{d}_k - \mathbf{C}_k\mathbf{x}_k^f), \tag{7}$$

$$\hat{\mathbf{P}}_k = [\mathbf{I} - \mathbf{K}_k\mathbf{C}_k]\mathbf{P}_k. \tag{8}$$

Linearizing $\boldsymbol{\Psi}_k$ about $\mathbf{x}_k^a$, we obtain

$$\boldsymbol{\Psi}_k(\mathbf{x}_k,\mathbf{f}_k) \approx \boldsymbol{\Psi}_k(\mathbf{x}_k^a,\mathbf{f}_k) + \boldsymbol{\Psi}_k'(\mathbf{x}_k^a,\mathbf{f}_k)(\mathbf{x}_k - \mathbf{x}_k^a). \tag{9}$$

$\boldsymbol{\Psi}_k'(\mathbf{x}_k,\mathbf{f}_k)$ denotes the tangent linear operator, being the Jacobian matrix of $\boldsymbol{\Psi}_k(\mathbf{x}_k,\mathbf{f}_k)$ with respect to $\mathbf{x}_k$.

Eqs. (4) and (9) lead to

$$\mathbf{x}_{k+1} = \boldsymbol{\Psi}_k(\mathbf{x}_k^a,\mathbf{f}_k) + \boldsymbol{\Psi}'k(\mathbf{x}_k^a,\mathbf{f}_k)(\mathbf{x}_k - \mathbf{x}_k^a) + \mathbf{q}_k. \tag{10}$$

From Eq. (10), one obtains the posterior mean and error covariance matrix [7,31,46,47] which constitutes the forecast step:

Forecast step:

$$\mathbf{x}_{k+1}^f = \boldsymbol{\Psi}_k(\mathbf{x}_k^a,\mathbf{f}_k), \tag{11}$$

$$\mathbf{P}_{k+1} = [\boldsymbol{\Psi}_k'(\mathbf{x}_k^a,\mathbf{f}_k)]\hat{\mathbf{P}}_k[\boldsymbol{\Psi}_k'(\mathbf{x}_k^a,\mathbf{f}_k)]^{\mathrm{T}} + \mathbf{Q}_k. \tag{12}$$

4. Ensemble Kalman filter

For a strongly nonlinear system, the extended Kalman filter may fail to provide acceptable conditional mean and covariance estimates due to linearization of the model operator. The ensemble Kalman filter partially addresses this issue in the context of strongly nonlinear systems (e.g. [7,31]). In the ensemble Kalman filter, the probability density function of the state vector is approximated using a finite number of Monte Carlo samples, known as ensemble members. In contrast to the extended Kalman filter, each ensemble member is integrated forward in time using the full nonlinear model which captures some or most of the non-Gaussian features in the state vector. However, the linear analysis step performed in the extended Kalman filter is kept intact offering computational efficiency. In brief, the ensemble Kalman filter algorithm can be summarized as follows [7]:

(1) Create an ensemble $\{\mathbf{x}_{0,i}^f\}$, $i=1,\ldots,N$, using the initial probability density function of $\mathbf{x}_0$.
(2) For each subsequent step, obtain the perturbed measurements and estimated measurement error covariance matrix:

$$\mathbf{d}_{k,i} = \mathbf{d}_k + \boldsymbol{\varepsilon}_{k,i}, \tag{13}$$

$$\boldsymbol{\Gamma}_k = \frac{1}{N-1}\sum_{j=1}^{N} \boldsymbol{\varepsilon}_{k,j}\boldsymbol{\varepsilon}_{k,j}^{\mathrm{T}}. \tag{14}$$

(3) *Analysis step*:

$$\mathbf{K}_k = \mathbf{P}_k\mathbf{C}_k^{\mathrm{T}}[\boldsymbol{\Gamma}_k + \mathbf{C}_k\mathbf{P}_k\mathbf{C}_k^{\mathrm{T}}]^{-1}, \tag{15}$$

$$\mathbf{x}_{k,i}^a = \mathbf{x}_{k,i}^f + \mathbf{K}_k(\mathbf{d}_{k,i} - \mathbf{C}_k\mathbf{x}_{k,i}^f), \tag{16}$$

$$\hat{\mathbf{P}}_k = [\mathbf{I} - \mathbf{K}_k\mathbf{C}_k]\mathbf{P}_k. \tag{17}$$

(4) *Forecast step*:

$$\mathbf{x}_{k+1,i}^f = \boldsymbol{\Psi}_k(\mathbf{x}_{k,i}^a, \mathbf{f}_k) + \mathbf{q}_{k,i}, \tag{18}$$

$$\hat{\mathbf{x}}_{k+1}^f = \frac{1}{N}\sum_{j=1}^{N} \mathbf{x}_{k+1,j}^f, \tag{19}$$

$$\mathbf{P}_{k+1} = \frac{1}{N-1}\sum_{j=1}^{N}(\mathbf{x}_{k+1,j}^f - \hat{\mathbf{x}}_{k+1}^f)(\mathbf{x}_{k+1,j}^f - \hat{\mathbf{x}}_{k+1}^f)^{\mathrm{T}}. \tag{20}$$

The linear analysis step in the ensemble Kalman filter is the major limitation for strongly nonlinear models, as it assumes a Gaussian prior probability density function which does not generally hold good for nonlinear models. Burgers, van Leeuwen and Evensen [21] and Whitaker and Hamill [48] reported the necessity of perturbing the measurements as in Eq. (13) to prevent underestimation of the error covariance matrix. The ensemble Kalman filter also eliminates the need to obtain the tangent linear operator as required by the extended Kalman filter. Furthermore, the ensemble Kalman filter avoids the memory-intensive explicit storage of the conditional covariance matrix $\mathbf{P}_{k+1}$ as required for the extended Kalman filter. In the ensemble Kalman filter, the forecast covariance matrix $\mathbf{P}_{k+1}$ is estimated using statistical averaging, as in Eq. (20).

The above formulation can be extended to handle multiplicative measurement noise through linearization of the measurement operator (e.g. [20]). Furthermore, the case of nonlinear measurement operator with additive noise can be tackled by augmenting the state vector with the nonlinear measurement term. In that case, the measurement becomes a linear function of the new augmented state vector, which bypasses the linearization step [49].

5. Particle filter

The mathematical formulation presented in this Section closely follows Tanizaki [39]. The most general representation of the evolution and measurement equations of a nonlinear dynamical system is

$$\mathbf{x}_{k+1} = \mathbf{g}_k(\mathbf{x}_k, \mathbf{f}_k, \mathbf{q}_k), \tag{21}$$

$$\mathbf{d}_k = \mathbf{h}_k(\mathbf{x}_k, \boldsymbol{\varepsilon}_k), \tag{22}$$

where $\mathbf{q}$ and $\boldsymbol{\varepsilon}$ are independent zero-mean random vectors which denote model and measurement errors, respectively, and $\mathbf{f}$ is a deterministic forcing vector. Let us define the set of state and the measurement vectors collectively as

$$\mathbf{X}_k = \{\mathbf{x}_0, \mathbf{x}_1, \ldots, \mathbf{x}_k\}, \tag{23}$$

$$\mathbf{D}_k = \{\mathbf{d}_0, \mathbf{d}_1, \ldots, \mathbf{d}_k\}. \tag{24}$$

By Bayes' Theorem [39], the conditional probability density function of $\mathbf{X}_k$ is given by

$$p(\mathbf{X}_k|\mathbf{D}_k) = \frac{p(\mathbf{D}_k|\mathbf{X}_k)p(\mathbf{X}_k)}{\int p(\mathbf{D}_k|\mathbf{X}_k)p(\mathbf{X}_k)\,\mathrm{d}\mathbf{X}_k}. \tag{25}$$

Consequently, the marginal conditional probability density function of $\mathbf{x}_k$ is given by

$$p(\mathbf{x}_k|\mathbf{D}_k) = \frac{\int p(\mathbf{D}_k|\mathbf{X}_k)p(\mathbf{X}_k)\,\mathrm{d}\mathbf{X}_{k-1}}{\int p(\mathbf{D}_k|\mathbf{X}_k)p(\mathbf{X}_k)\,\mathrm{d}\mathbf{X}_k}. \tag{26}$$

Therefore, the conditional mean of the state vector $\mathbf{x}$ is

$$\hat{\mathbf{x}}_k = \int \mathbf{x}_k p(\mathbf{x}_k|\mathbf{D}_k)\,\mathrm{d}\mathbf{x}_k = \frac{\int \mathbf{x}_k p(\mathbf{D}_k|\mathbf{X}_k)p(\mathbf{X}_k)\,\mathrm{d}\mathbf{X}_k}{\int p(\mathbf{D}_k|\mathbf{X}_k)p(\mathbf{X}_k)\,\mathrm{d}\mathbf{X}_k}. \tag{27}$$

Clearly, $\mathbf{d}_k$ depends only on $\mathbf{x}_k$ defined by Eq. (22). This fact permits the following expression of $p(\mathbf{D}_k|\mathbf{X}_k)$

$$p(\mathbf{D}_k|\mathbf{X}_k) = \prod_{s=0}^{k} p(\mathbf{d}_s|\mathbf{x}_s). \tag{28}$$

The mean in Eq. (27) can be statistically approximated using N random samples of $\mathbf{X}_k$ as

$$\hat{\mathbf{x}}_k \approx \frac{\frac{1}{N}\sum_{i=1}^{N} \mathbf{x}_{k,i} p(\mathbf{D}_k|\mathbf{X}_{k,i})}{\frac{1}{N}\sum_{j=1}^{N} p(\mathbf{D}_k|\mathbf{X}_{k,j})} = \sum_{i=1}^{N} w_{k,i}\mathbf{x}_{k,i}, \tag{29}$$

where

$$w_{k,i} = \frac{p(\mathbf{d}_k|\mathbf{x}_{k,i})w_{k-1,i}}{\sum_{j=1}^{N} p(\mathbf{d}_k|\mathbf{x}_{k,j})w_{k-1,j}}. \tag{30}$$

In summary, the particle filter can be implemented using the following algorithm:

(1) Draw N samples $\mathbf{x}_{0,i}$ using $p(\mathbf{x}_0)$, $i = 1, \ldots, N$.
(2) Set $w_{0,i} = 1/N$.
(3) Perform the following steps consecutively:
  (a) Obtain $\mathbf{x}_{k,i}$ from $\mathbf{x}_{k-1,i}$ for each value of i using Eq. (21).
  (b) Obtain $w_{k,i}$ for each value of i using Eq. (30).
  (c) Compute the estimate of $\mathbf{x}_k$ using Eq. (29).

As alluded to previously, the particle filter can estimate the state of the system given general forms of nonlinearities in measurement and model operators and non-Gaussian model and measurement errors. In contrast to the extended Kalman filter and ensemble Kalman filter, no Gaussian approximation of the system state is made at any stage in the particle filter. Therefore, the particle filter is superior to the ensemble Kalman filter and extended Kalman filter for strongly non-Gaussian models. The particle filter is based on non-parametric statistics and directly deals with the estimation of the probability density function of state vector, without any assumption on the form of probability density function. For an infinitely large ensemble, the estimates provided by the particle filter asymptotically reach the exact solution for Eq. (3). The ensemble Kalman filter, by contrast, may lead to erroneous state estimates even in the limit of infinitely large ensembles due to the Gaussian closure in the analysis step.

The particle filter in general requires larger ensemble sizes to obtain reasonably accurate estimates of the system state and may become impractical for large scale systems due to intensive computational requirements. Depending on the non-Gaussian trends in the conditional probability density function, the ensemble Kalman filter offers an alternative which may prove to be computationally expedient. The requirement for larger ensembles can be partly alleviated by adopting a resampling step and an efficient sampling technique, such as latin hypercube sampling [50,51], as adopted in this paper.

5.1. Resampling

In certain cases, the particle filter may experience the so-called degeneracy phenomenon [31,35]. In this situation, only one particle has significant weight after a certain amount of data is assimilated using the particle filter. The computational resources expended in propagating the particles with negligible weights are wasted as these particles make little or no contribution to the state estimate. One suitable measure of degeneracy is the effective sample size given by [31,35]

$$N_{\text{eff}} = \frac{1}{\sum_{i=1}^{N} (w_{k,i})^2}. \tag{31}$$

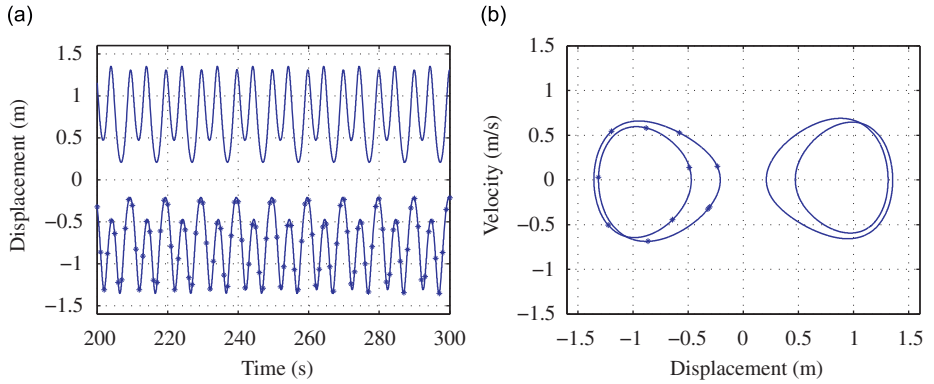

Fig. 1. Response of the Duffing oscillator under purely deterministic input with $\mathcal{T} = 0.3$, $\sigma = 0$: (a) two steady-state trajectories and (b) the associated phase–space diagrams.

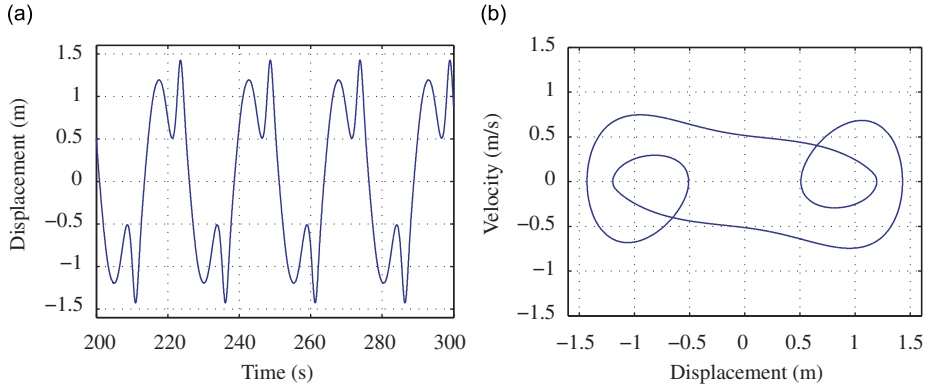

Fig. 2. Response of the Duffing oscillator under purely deterministic input with $\mathcal{T} = 0.37$, $\sigma = 0$: (a) steady-state trajectory and (b) the associated phase–space diagram.

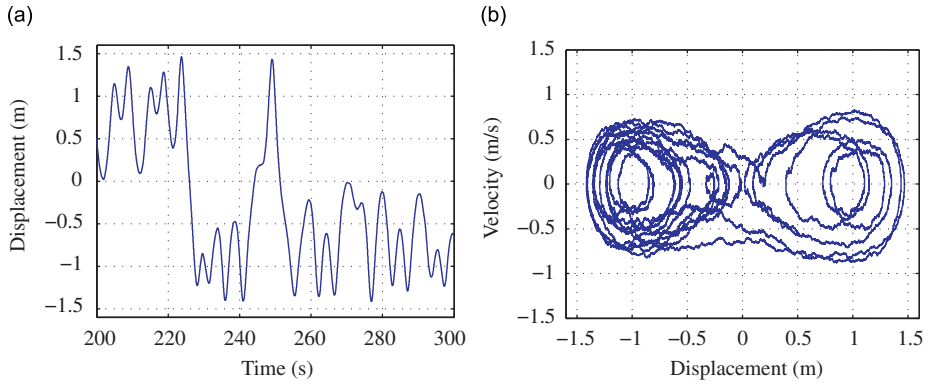

Fig. 3. Response of the Duffing oscillator under combined deterministic and random input with $\mathcal{T} = 0.3$, $\sigma = 0.1$: (a) steady-state trajectory and (b) the associated phase–space diagram.

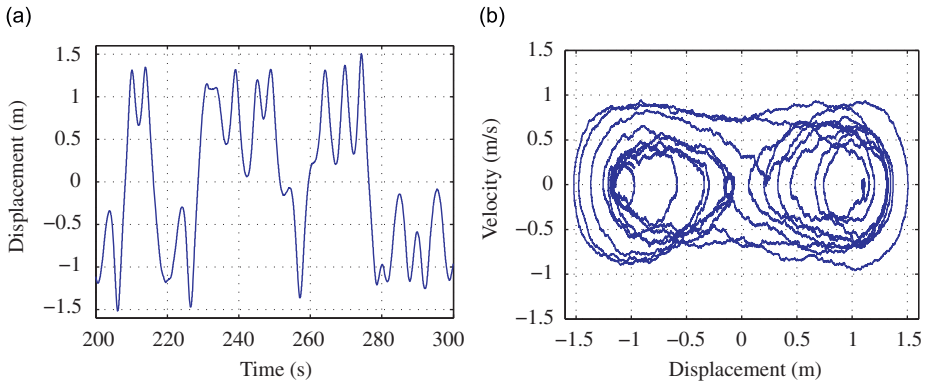

Fig. 4. Response of the Duffing oscillator under combined deterministic and random input with $\mathcal{T} = 0.37$, $\sigma = 0.1$: (a) steady-state trajectory and (b) the associated phase–space diagram.

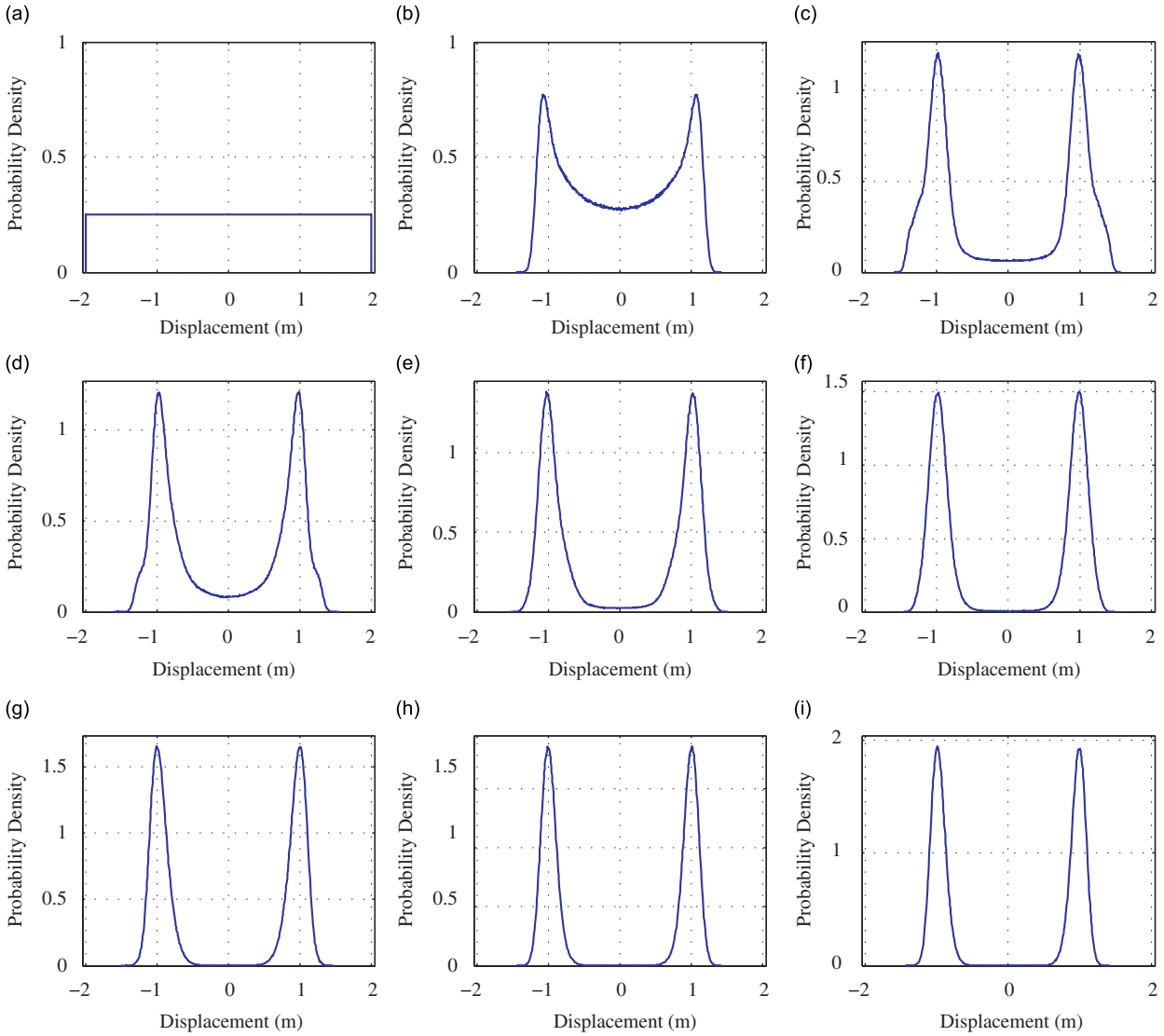

Fig. 5. Transition probability density function of the system under purely random input with $\sigma = 0.1$ and $\mathcal{T} = 0$: (a) initial uniform probability density function; (b) probability density at $t = 2$ time units; (c) probability density at $t = 4$ time units; (d) probability density at $t = 6$ time units; (e) probability density at $t = 8$ time units; (f) probability density at $t = 10$ time units; (g) probability density at $t = 12$ time units; (h) probability density at $t = 14$ time units; and (i) probability density at $t = 16$ time units.

One can detect the degeneracy phenomenon when $N_{\text{eff}} < N_{\text{thr}}$, where N_{thr} is the threshold value. When such degeneracy condition is encountered, a resampling from the conditional probability density function is carried out:

(1) Sample N particles from the current pool of particles with probabilities equal to their weights $w_{k,i}$.
(2) Replacing the current particle set with the new one obtained above.
(3) Reset the weights as $w_{k,i} = 1/N$, for $i = 1, \ldots, N$.

6. Noisy limit cycle oscillation of a Duffing system

For numerical illustration, we consider a Duffing oscillator undergoing limit cycle oscillation. In this section, we investigate the performance of the extended Kalman filter, ensemble Kalman filter and particle filter in tracking limit cycle oscillations using numerical data. In particular, we examine the influence of measurement and model noise and sparsity of observational data on the tracking capabilities of the extended Kalman filter, ensemble Kalman filter and particle filter.

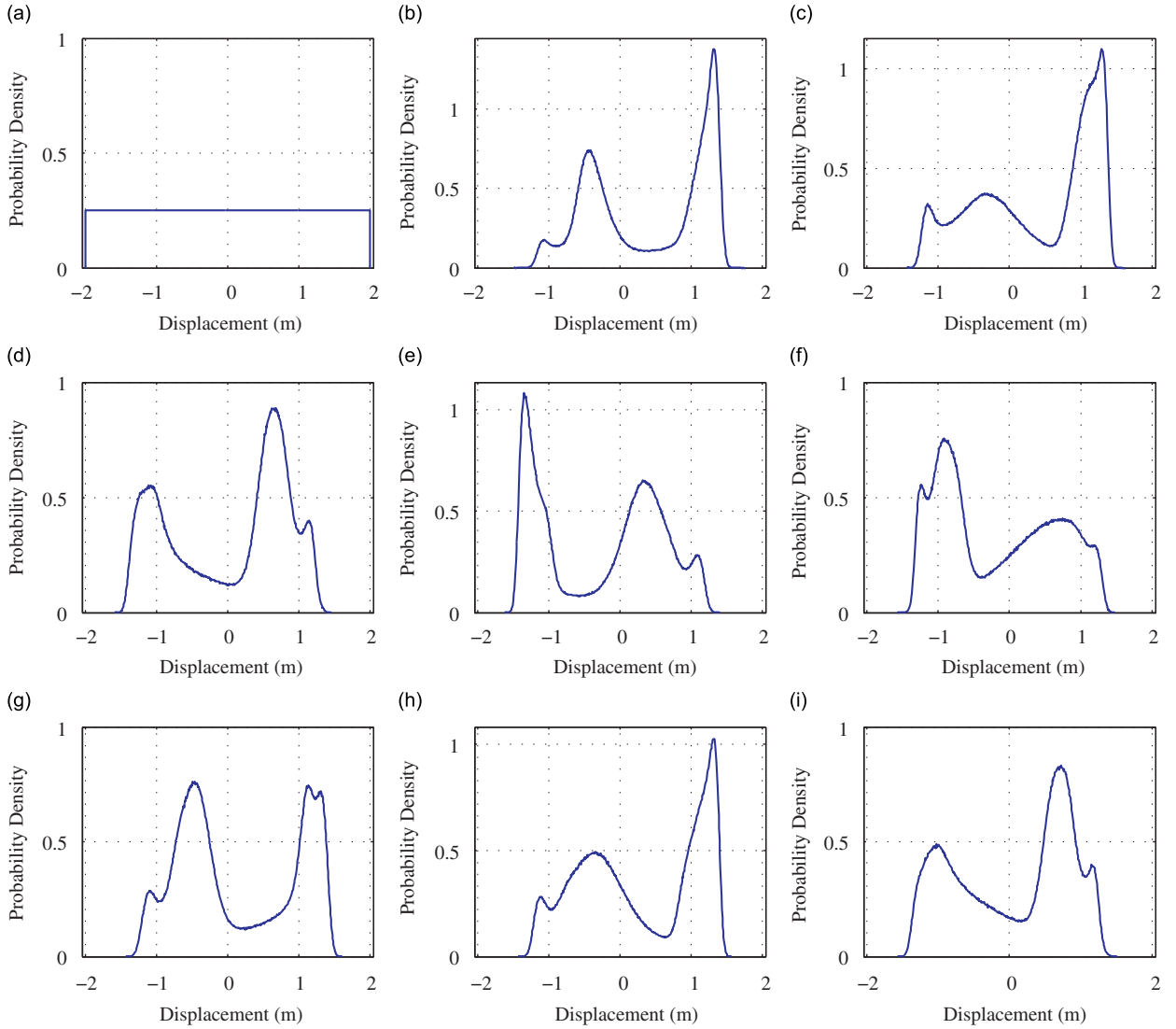

Fig. 6. Transition probability density function of the system under combined deterministic and random input with $\sigma = 0.1$ and $\mathcal{T} = 0.3$: (a) initial uniform probability density function; (b) probability density at $t = 6$ time units; (c) probability density at $t = 12$ time units; (d) probability density at $t = 18$ time units; (e) probability density at $t = 24$ time units; (f) probability density at $t = 30$ time units; (g) probability density at $t = 36$ time units; (h) probability density at $t = 42$ time units; and (i) probability density at $t = 48$ time units.

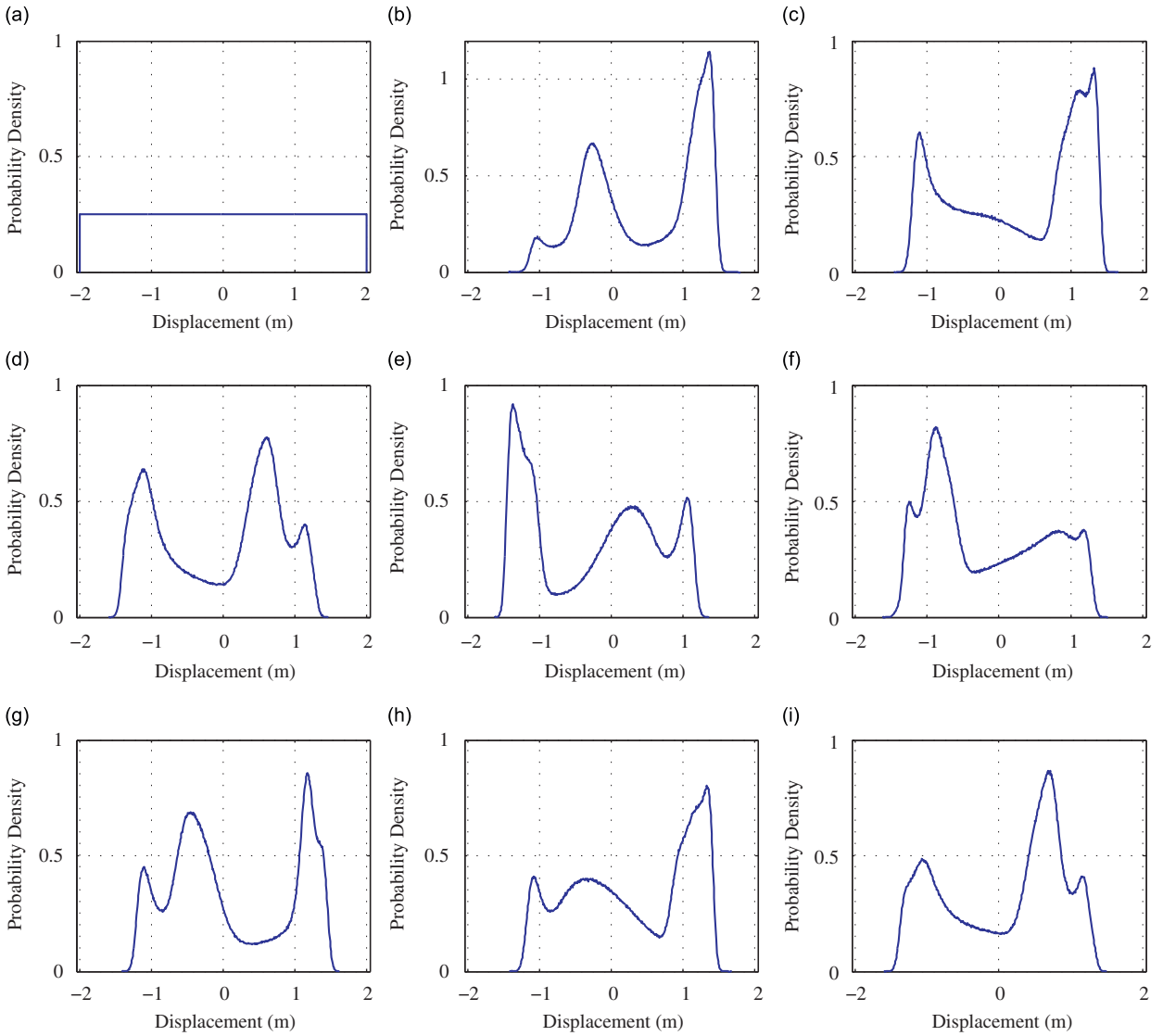

Fig. 7. Transition probability density function of the system under combined deterministic and random input with $\sigma = 0.1$ and $\mathcal{T} = 0.37$: (a) initial uniform probability density function; (b) probability density at $t = 6$ time units; (c) probability density at $t = 12$ time units; (d) probability density at $t = 18$ time units; (e) probability density at $t = 24$ time units; (f) probability density at $t = 30$ time units; (g) probability density at $t = 36$ time units; (h) probability density at $t = 42$ time units; and (i) probability density at $t = 48$ time units.

6.1. *Duffing oscillator model*

The equation of motion of a Duffing oscillator subjected to combined deterministic and random inputs is described as (e.g. [52,53]):

$$\ddot{u}(t) + c\dot{u}(t) + k_1 u(t) + k_3 u^3(t) = \mathcal{T}\cos(\omega t) + \sigma\xi(t). \tag{32}$$

Here, c is the damping coefficient, k_1 and k_3 are the linear and nonlinear stiffness coefficients, $u(t)$ is the displacement, $\mathcal{T}$ and ω are the amplitude and frequency of the sinusoidal input, $\xi(t)$ is a Gaussian white noise describing the random input and σ denotes its strength.

Despite its mathematical simplicity, the Duffing system displays a wide range of dynamics from periodic to chaotic motion with a slight change in its model parameters. For instance, when a Duffing system exhibits a double-well potential function for its autonomous counterpart, qualitatively different limit cycle oscillations emerge by slight variations in the

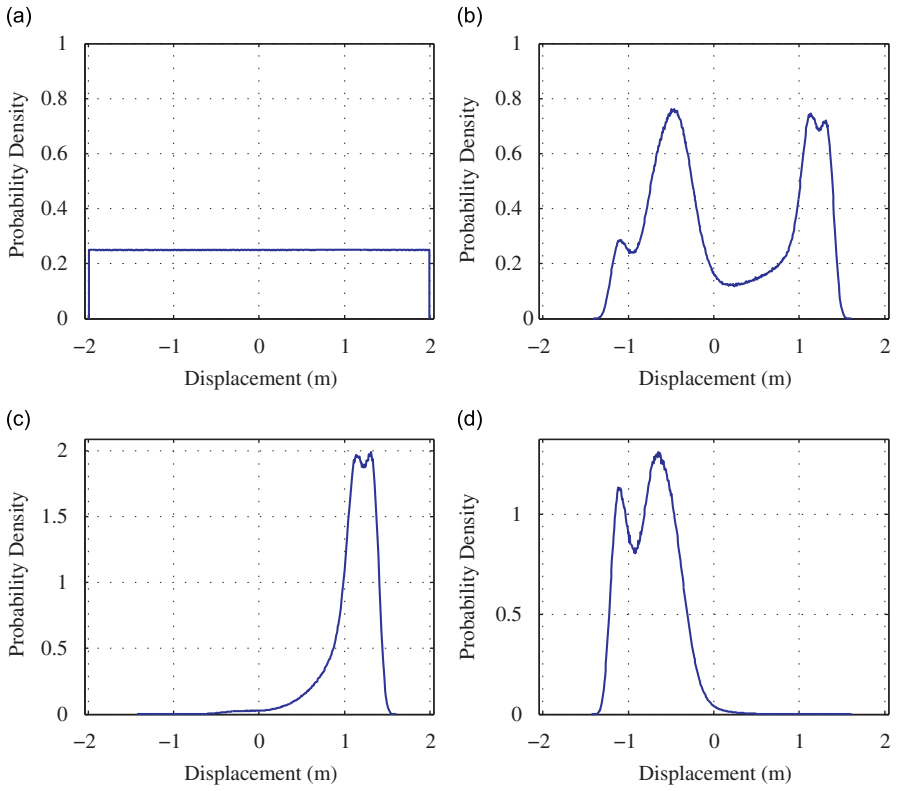

Fig. 8. Conditional probability density function of the system with $\sigma = 0.1$ and $\mathcal{T} = 0.3$: (a) initial uniform probability density function; (b) prior probability density at $t = 36$ time units; (c) conditional probability density given measurement $d_k = 1.3$; and (d) conditional probability density given measurement $d_k = -1.3$.

amplitude of the harmonic input $\mathcal{T}$ for the forced system.[1] These facts prompted the use of the Duffing oscillator as a paradigm model in this investigation.

Using nonlinear filtering techniques, we are primarily interested in tracking the noisy limit cycle oscillation of the Duffing oscillator from a set of noisy observational data obtained at discrete times t_k:

$$d_k = u(t_k) + \varepsilon_k. \tag{33}$$

Before we discuss the tracking problem using nonlinear filters, let us rewrite Eq. (32) in the state-space form as

$$\dot{x}_1 = x_2, \tag{34}$$

$$\dot{x}_2 = -[cx_2 + k_1x_1 + k_3x_1^3] + \mathcal{T}\cos(\omega t) + \sigma\xi(t), \tag{35}$$

where $x_1 = u$ and $x_2 = \dot{u}$. The following Itô stochastic differential equations describe the above system represented by Eqs. (34) and (35)

$$\mathrm{d}x_1 = x_2\,\mathrm{d}t, \tag{36}$$

$$\mathrm{d}x_2 = -[cx_2 + k_1x_1 + k_3x_1^3 - \mathcal{T}\cos(\omega t)]\,\mathrm{d}t + \sigma\xi(t)\,\mathrm{d}t, \tag{37}$$

where $\xi(t)\,\mathrm{d}t = \mathrm{d}W = W(t_{k+1}) - W(t_k)$ is the Brownian path increment.

The discrete representation the above Itô stochastic differential equation using the Euler–Maruyama stochastic integration scheme [54] with time step Δt provides the following discrete state-evolution equations:

$$\{x_1\}_{k+1} = \{x_1\}_k + \Delta t\{x_2\}_k, \tag{38}$$

$$\{x_2\}_{k+1} = \{x_2\}_k - \Delta t[c\{x_2\}_k + k_1\{x_1\}_k + k_3\{x_1\}_k^3 - \mathcal{T}\cos(\omega t_k)] + \sigma\,\mathrm{d}W. \tag{39}$$

[1] In the engineering literature, limit cycle oscillation generally denotes a periodic motion that arises from an autonomous system. In the dynamical systems literature, limit cycle oscillation also includes forced periodic motion [4]. The response of a forced Duffing oscillator has been described as a limit cycle oscillation in [3].

6.2. Limit cycle oscillation of the Duffing oscillator

Next we investigate the limit cycle oscillation of the Duffing system. In particular, we examine only two subharmonic limit cycle oscillations as described later in this section. The following numerical values of the system parameters are considered [52,53]: $c = 0.3$, $k_1 = -1$, $k_3 = 1$, $\omega = 1.25$ and $\Delta t = 5 \times 10^{-4}$. For this parameter set, the autonomous (unforced) system has three fixed points. The fixed point at $u = 0$ is unstable, while the two fixed points at ± 1 are stable. Figs. 1 and 2 display the steady-state displacement u and its phase–space diagram under purely deterministic loading ($\sigma = 0$) for $\mathcal{T} = 0.3$ and 0.37, respectively. The two trajectories in Fig. 1 represent the steady state limit cycle oscillations about the stable fixed points, starting with different initial conditions. In the absence of modelling noise ($\sigma = 0$), when $\mathcal{T} = 0.3$, the system exhibits a period-two subharmonic limit cycle oscillation with period $4\pi/\omega$. On the other hand, a period-five subharmonic limit cycle oscillation with period $10\pi/\omega$ appears for $\mathcal{T} = 0.37$. Due to phenomenologically different vibration features, we have considered these two values of $\mathcal{T}$ throughout the paper. It is expected that these two values of $\mathcal{T}$ would give a fairly complete picture of the underlying issues with minimal numerical illustrations.

Figs. 3 and 4 present sample trajectories and the associated phase–space diagrams of the noisy limit cycle oscillations perturbed by relatively strong random noise ($\sigma = 0.1$) with $\mathcal{T} = 0.3$ and 0.37, respectively. Note that the transient response associated with the initial conditions is not shown. Under such strong random perturbation, the limit cycle oscillations become highly irregular as evident in the phase–space diagrams in Figs. 3 and 4. However, the two cases of limit cycle oscillation examined still show differences in that $\mathcal{T} = 0.37$ results in more frequent basin hopping in comparison to $\mathcal{T} = 0.3$, as evident in the time responses shown in Figs. 3 and 4.

6.3. Transition probability density function of limit cycle oscillation

The transition probability density function of the system driven purely by random noise ($\mathcal{T} = 0$ and $\sigma = 0.1$) is shown in Fig. 5 with initial conditions $x_1 \sim \mathrm{U}[-2, 2]$ and $x_2 = 0$. The transition probability density function is obtained using 6×10^6 Monte Carlo samples running in parallel on a distributed-memory multiprocessor machine (HP Intel Xeon cluster with 178 processor cores) using message-passing interface (MPI) [55]. To expedite the statistical convergence with fewer samples, latin hypercube sampling was employed as an efficient sampling technique. Latin hypercube sampling achieves greater

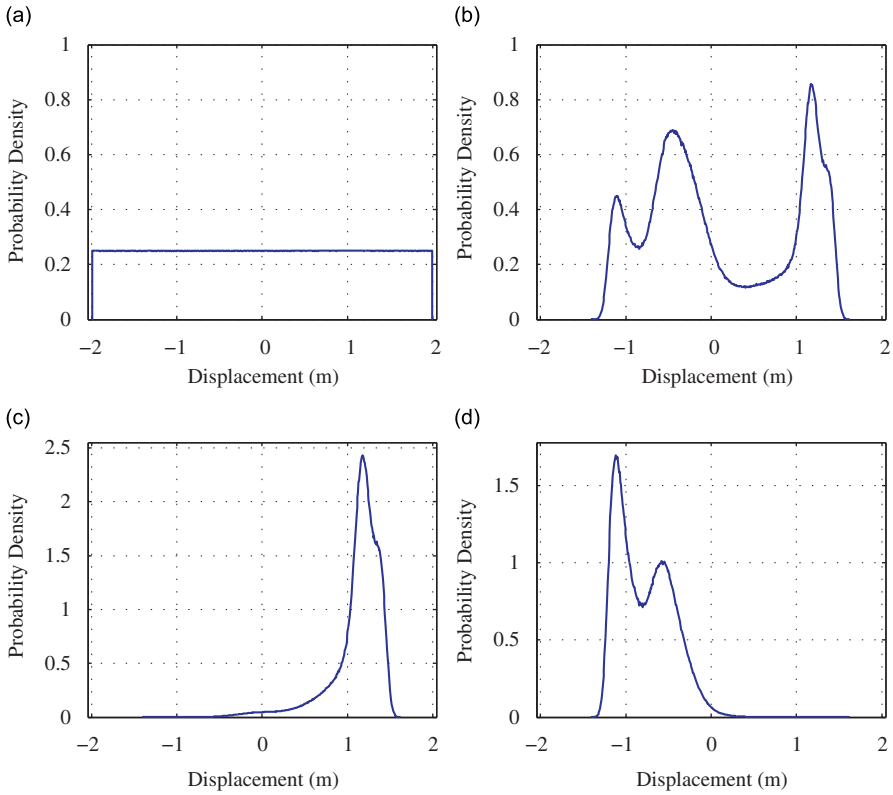

Fig. 9. Conditional probability density of the system with $\sigma = 0.1$ and $\mathcal{T} = 0.37$: (a) initial uniform probability density function; (b) prior probability density at $t = 36$ time units; (c) conditional probability density given measurement $d_k = 1.3$; and (d) conditional probability density given measurement $d_k = -1.3$.

efficiency than simple random sampling by picking samples in a democratic fashion from a given probability density function. Latin hypercube sampling ensures that the generated ensemble is representative of the real probability density function for a specific ensemble size, whereas the simple random sampling provides no guarantees (more details can be found in [50,51] for example). The initial uniform probability density function of x_1 converges to a bimodal (strongly non-Gaussian) stationary distribution having dominant peaks at the stable fixed points $u = \pm 1$.

Next we turn our attention to the forced system. The transition probability density functions of the displacement x_1 are plotted in Figs. 6 and 7 under combined deterministic and random excitations ($\sigma = 0.1$) for two noisy limit cycle oscillations. The transition probability density function are generated using 6×10^6 random samples using latin hypercube sampling. Initial conditions are $x_1 \sim U[-2, 2]$ and $x_2 = 0$. The strongly non-Gaussian trends in the transition probability density functions are clearly evident in both Figs. 6 and 7. In Fig. 5, the probability mass is centered around the two stable fixed points $u = \pm 1$. This is due to the fact that the oscillation is predominantly confined in the neighborhood of potential wells around $u = \pm 1$. By contrast, about three to four sharp peaks appear in the transition probability density functions shown in Figs. 6 and 7.

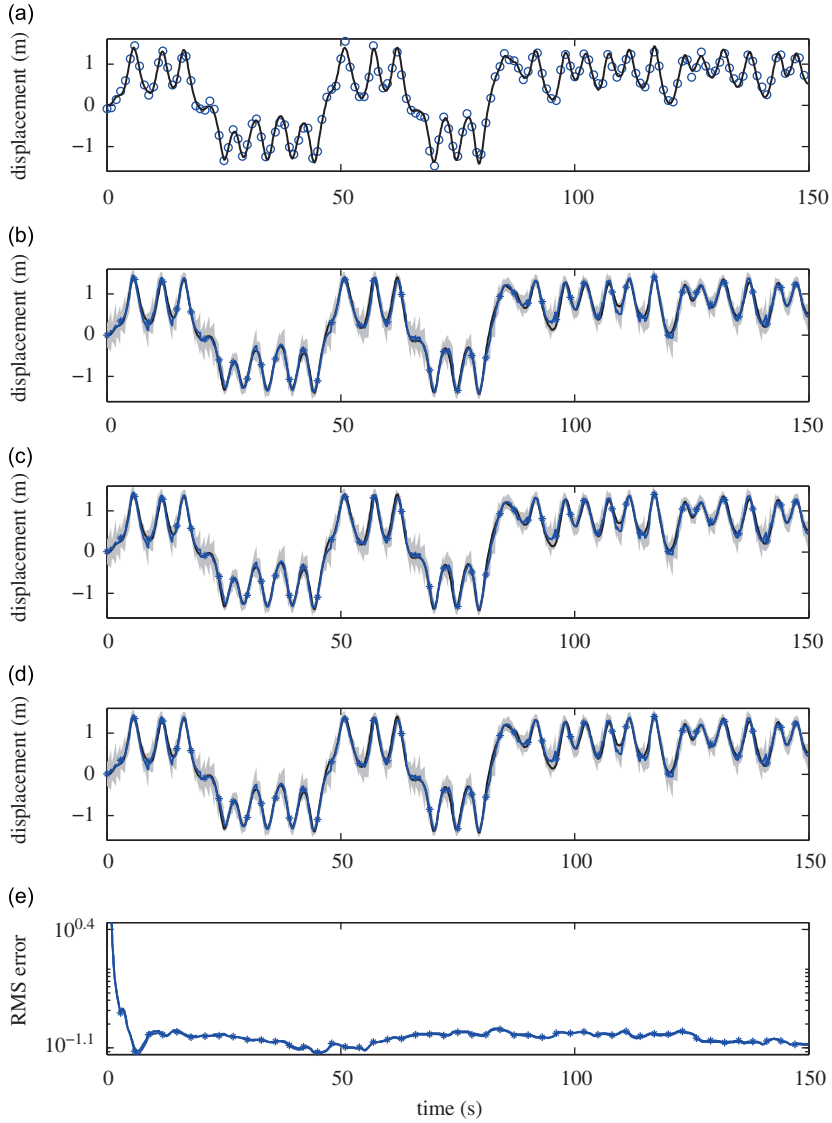

Fig. 10. True, measured and estimated displacement of the Duffing oscillator for $\mathcal{T} = 0.3$: (a) true (solid line) and measured (circles) displacement; (b) extended Kalman filter estimate (blue line with stars) ± 3 error standard deviations (light blue area); (c) ensemble Kalman filter estimate (blue line with stars) ± 3 error standard deviations (light blue area) with $N = 50$; (d) particle filter estimate (blue line with stars) ± 3 error standard deviations (light blue area) with $N = 50$; and (e) time-averaged normalized root-mean-square estimate errors of the extended Kalman filter (dashed line), ensemble Kalman filter (solid line) and particle filter (solid line with stars). (For interpretation of the references to color in this figure legend, the reader is referred to the web version of this article.)

Nonlinear filtering techniques estimate the conditional probability density functions of the system given noisy observational data. The effective performance of these filters relies heavily on the characteristics of the conditional probability density functions. For example, strong non-Gaussian features in the conditional probability density functions diminishes the efficacy of the extended Kalman filter. On the contrary, the particle filter is robust to non-Gaussian trends. It is therefore instructive to focus on the nature of the conditional probability density function to judiciously apply nonlinear filters. Some examples of the conditional probability density functions are presented in the bottom panels of Figs. 8 and 9 using two measurements $d_k = \pm 1.3$ corrupted by Gaussian noise for $\mathcal{T} = 0.3$ and 0.37, respectively. The variance of the zero-mean Gaussian measurement noise is taken to be 0.3. The initial and transition probability density functions are shown in the top panels of Figs. 8 and 9. Strong non-Gaussian features in the conditional probability density functions are clearly evident which point out the need to use nonlinear filtering techniques such as the ensemble Kalman filter and particle filter.

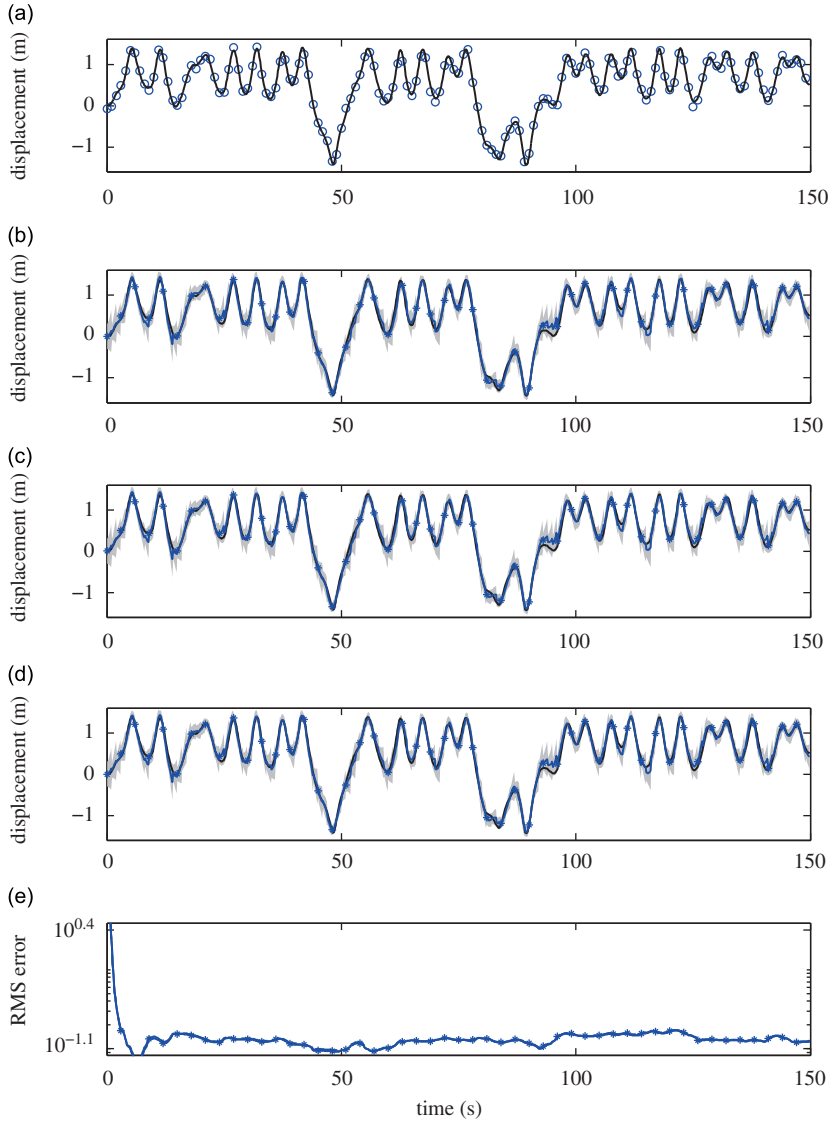

Fig. 11. True, measured and estimated displacement of the Duffing oscillator for $\mathcal{T} = 0.37$: (a) true (solid line) and measured (circles) displacement; (b) extended Kalman filter estimate (blue line with stars) ± 3 error standard deviations (light blue area); (c) ensemble Kalman filter estimate (blue line with stars) ± 3 error standard deviations (light blue area) with $N = 50$; (d) particle filter estimate (blue line with stars) ± 3 error standard deviations (light blue area) with $N = 50$; and (e) time-averaged normalized root-mean-square estimate errors of the extended Kalman filter (dashed line), ensemble Kalman filter (solid line) and particle filter (solid line with stars). (For interpretation of the references to color in this figure legend, the reader is referred to the web version of this article.)

6.4. Tracking limit cycle oscillations

Next we conduct extensive numerical experiments related to tracking limit cycle oscillations using nonlinear filters. In Fig. 10, the top panel shows the displacement of the oscillator and the associated observational data d_k contaminated by Gaussian noise $\varepsilon_k \sim \mathcal{N}(0, 5.96 \times 10^{-3})$ for the case of $\mathcal{T} = 0.3$. For $\mathcal{T} = 0.37$, the true displacement and noisy measurements d_k polluted by Gaussian noise $\varepsilon_k \sim \mathcal{N}(0, 4.24 \times 10^{-3})$ are plotted in the top panel of Fig. 11. The standard deviation of the measurement noise is taken to be 10 percent of the root-mean-square (RMS) value of the true displacement. The modelling error has an amplitude of $\sigma = 0.1$. The observational data is acquired and analyzed at intervals of 1 time unit. For the ensemble Kalman filter and particle filter, an ensemble size of $N = 50$ is used. Furthermore, 200 independent experiments are performed for the ensemble Kalman filter and particle filter using the same measurement data. The averages of the mean and variance obtained from these experiments are plotted in Figs. 10 and 11. The averaging is performed to decrease statistical sampling errors in the estimates obtained from the ensemble Kalman filter and particle filter. To further

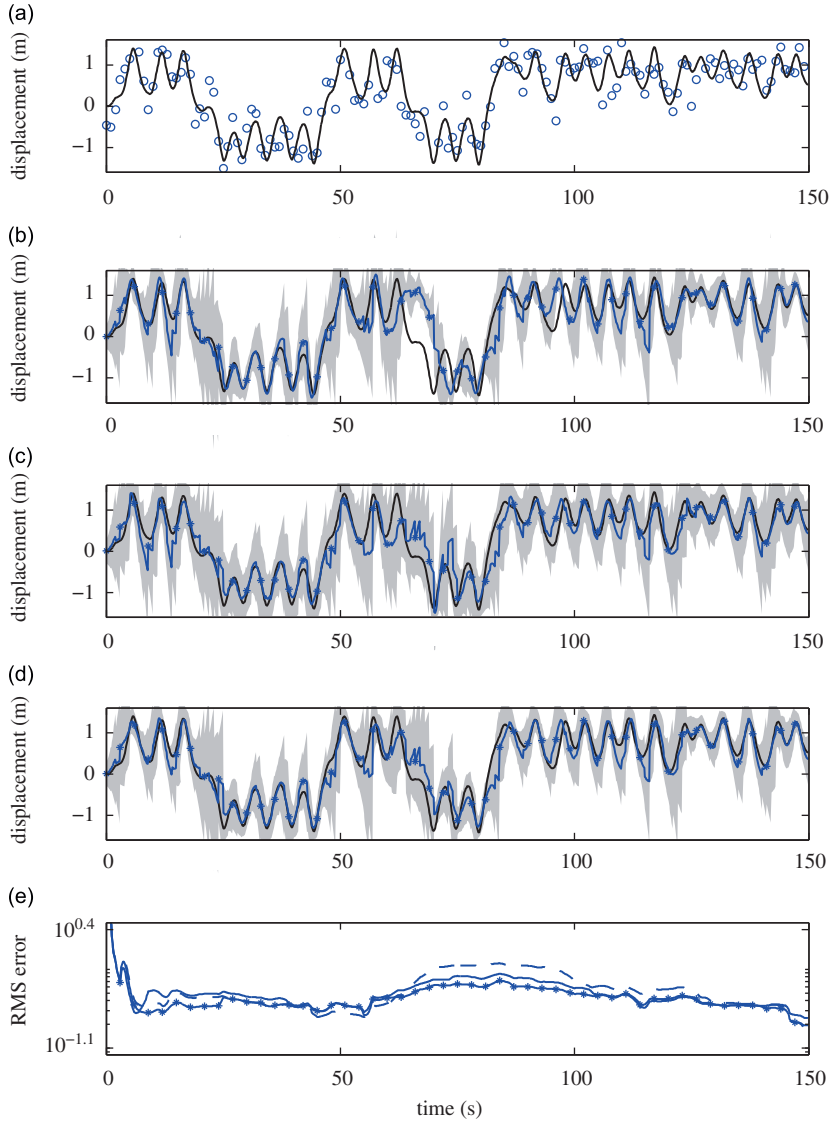

Fig. 12. True, measured and estimated displacement of the Duffing oscillator under stronger measurement noise for $\mathcal{T} = 0.3$: (a) true (solid line) and measured (circles) displacement; (b) extended Kalman filter estimate (blue line with stars) ± 3 error standard deviations (light blue area); (c) ensemble Kalman filter estimate (blue line with stars) ± 3 error standard deviations (light blue area) with $N = 50$; (d) particle filter estimate (blue line with stars) ± 3 error standard deviations (light blue area) with $N = 50$; and (e) time-averaged normalized root-mean-square estimate errors of the extended Kalman filter (dashed line), ensemble Kalman filter (solid line) and particle filter (solid line with stars). (For interpretation of the references to color in this figure legend, the reader is referred to the web version of this article.)

minimize sampling errors, latin hypercube sampling [50,51] is employed as an efficient sampling scheme by both the ensemble Kalman filter and particle filter.

Figs. 10 and 11 present the state estimation results using the extended Kalman filter (second panel from the top), ensemble Kalman filter (third panel from the top) and particle filter (fourth panel from the top). Initial conditions are $x_1 \sim \mathcal{N}(0.0, 0.1)$ and $x_2 \sim \mathcal{N}(0, 0.1)$. The moving average of the normalized RMS errors of the estimates are plotted in the bottom-most panel of Figs. 10 and 11. The error is normalized by the variance of the true displacement and the average is taken over the last fifteen time units. The threshold effective ensemble size for the particle filter for resampling purposes is chosen to be 75 percent of the ensemble size (i.e. $N_{\text{thr}} = 0.75N$). From the experience gained by the authors through numerical investigations, this value for the threshold ensemble size turned out to be adequate for effective resampling. The extended Kalman filter, ensemble Kalman filter and particle filter all provide comparable estimates. Furthermore, the small error covariance of the estimates is due to the frequent assimilation of data corrupted by small measurement noise. It is interesting to note that all three filters are capable of tracking the transition of the response from one potential well ($u = 1$) to the other ($u = -1$). Due to unstable dynamics, the standard deviation of the error in the estimates increases whenever the response trajectory approaches the fixed point ($u = 0$).

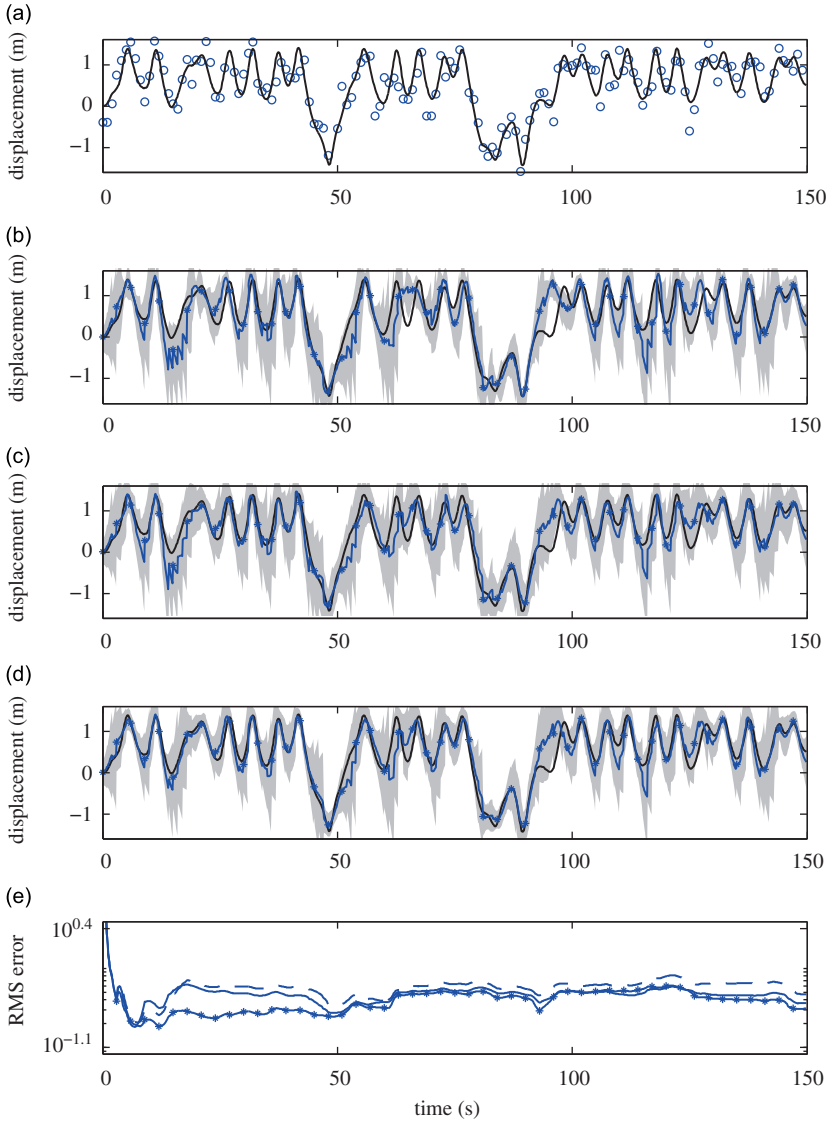

Fig. 13. True, measured and estimated displacement of the Duffing oscillator under stronger measurement noise for $\mathcal{T} = 0.37$: (a) true (solid line) and measured (circles) displacement; (b) extended Kalman filter estimate (blue line with stars) ± 3 error standard deviations (light blue area); (c) ensemble Kalman filter estimate (blue line with stars) ± 3 error standard deviations (light blue area) with $N = 50$; (d) particle filter estimate (blue line with stars) ± 3 error standard deviations (light blue area) with $N = 50$; and (e) time-averaged normalized root-mean-square estimate errors of the extended Kalman filter (dashed line), ensemble Kalman filter (solid line) and particle filter (solid line with stars). (For interpretation of the references to color in this figure legend, the reader is referred to the web version of this article.)

6.4.1. Effect of measurement noise

To demonstrate the effect of measurement noise on the state estimates, we consider the observational data acquired at every 1 time unit, same as in the previous experiment, but with stronger measurement noise, in contrast to the previous experiment. Fig. 12 shows the displacement of the oscillator for $\mathcal{T} = 0.3$ and the measured displacement d_k contaminated by Gaussian noise $\varepsilon_k \sim \mathcal{N}(0, 1.49 \times 10^{-1})$. Fig. 13 shows the displacement of the oscillator for $\mathcal{T} = 0.37$ along with the measured displacement d_k contaminated by Gaussian noise $\varepsilon_k \sim \mathcal{N}(0, 1.06 \times 10^{-1})$. The standard deviation of the measurement noise is taken to be 50 percent of the root-mean-square (RMS) value of the true displacement.

The state estimation results using the extended Kalman filter, the ensemble Kalman filter and particle filter are shown in the second, third and fourth panels from the top in Figs. 12 and 13, respectively. In relation to the results from the previous experiment shown in Figs. 10 and 11, it is evident that an increase in the strength of measurement noise deteriorates the accuracy of the estimates for all filters. The ensemble Kalman filter and particle filter provide similar results. The performance of the extended Kalman filter is the worst. It is believed that the superior performance of the ensemble Kalman filter and particle filter in this experiment is due to stronger non-Gaussian features in the conditional probability density function in comparison to the previous case. This maybe inferred, for instance, looking at the conditional

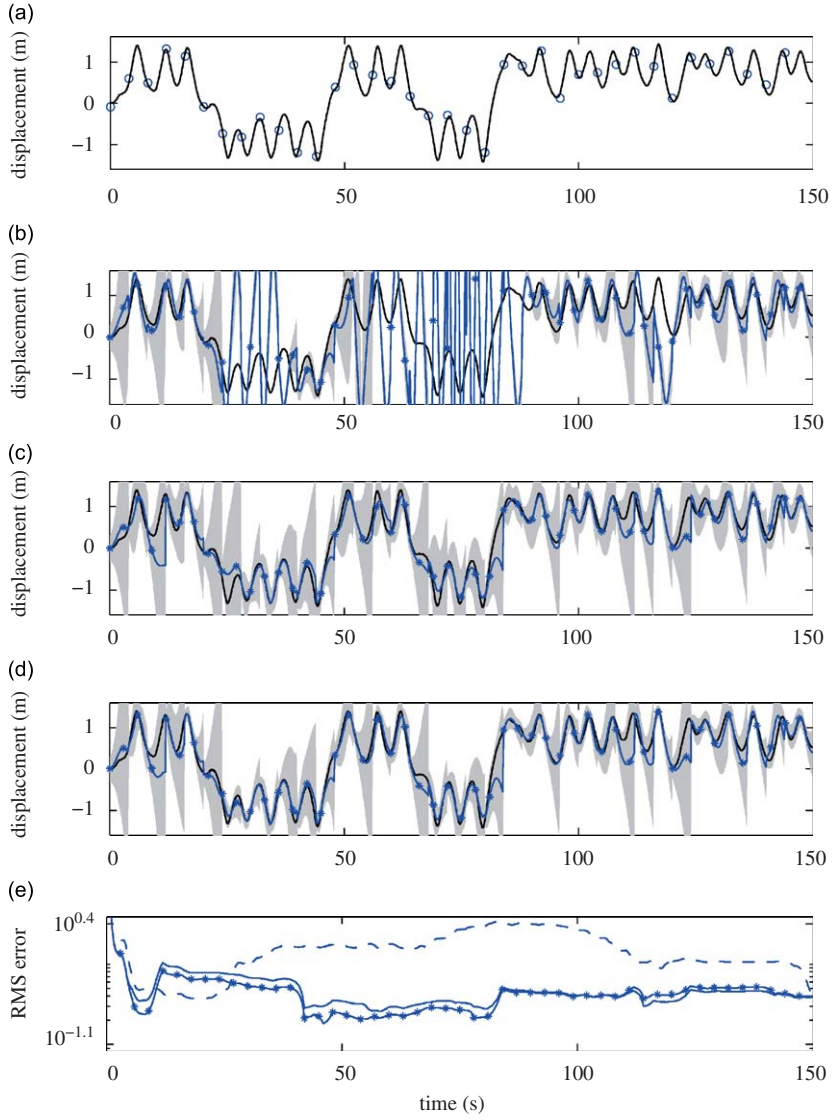

Fig. 14. True, measured and estimated displacement of the Duffing oscillator with sparse measurements for $\mathcal{T} = 0.3$: (a) true (solid line) and measured (circles) displacement; (b) extended Kalman filter estimate (blue line with stars) ± 3 error standard deviations (light blue area); (c) ensemble Kalman filter estimate (blue line with stars) ± 3 error standard deviations (light blue area) with $N = 50$; (d) particle filter estimate (blue line with stars) ± 3 error standard deviations (light blue area) with $N = 50$; and (e) time-averaged normalized root-mean-square estimate errors of the extended Kalman filter (dashed line), ensemble Kalman filter (solid line) and particle filter (solid line with stars). (For interpretation of the references to color in this figure legend, the reader is referred to the web version of this article.)

probability density functions plotted in Figs. 8 and 9 where the increase in measurement noise more effectively retains the non-Gaussian features in the posterior probability density function. In contrast to the previous case, the error standard deviation of the estimates is greater for all three filters. The increase in error standard deviation of the estimates is due to an increase in the variance of the measurement noise. The particle filter estimates display slightly smaller error covariances when compared to those of the extended Kalman filter which may be due to the resampling step undertaken in the particle filter.

6.4.2. *Effect of observational data sparsity*

In this subsection, we consider the case of sparse observational data. In particular, we consider observations obtained at time intervals of 4 time units, instead of 1 time unit used in the previous experiments. The standard deviation of measurement noise is 10 percent of that of the RMS value of the true displacement. The true and measured displacement are shown in the top most panel in Figs. 14 and 15. The state estimates of the extended Kalman filter, ensemble Kalman filter and particle filter are shown in subplots (b) through (d) in Figs. 14 and 15. Similar to the last experiment, the extended Kalman filter again leads to highly biased estimates due to an increase in data sparsity. The ensemble Kalman filter and

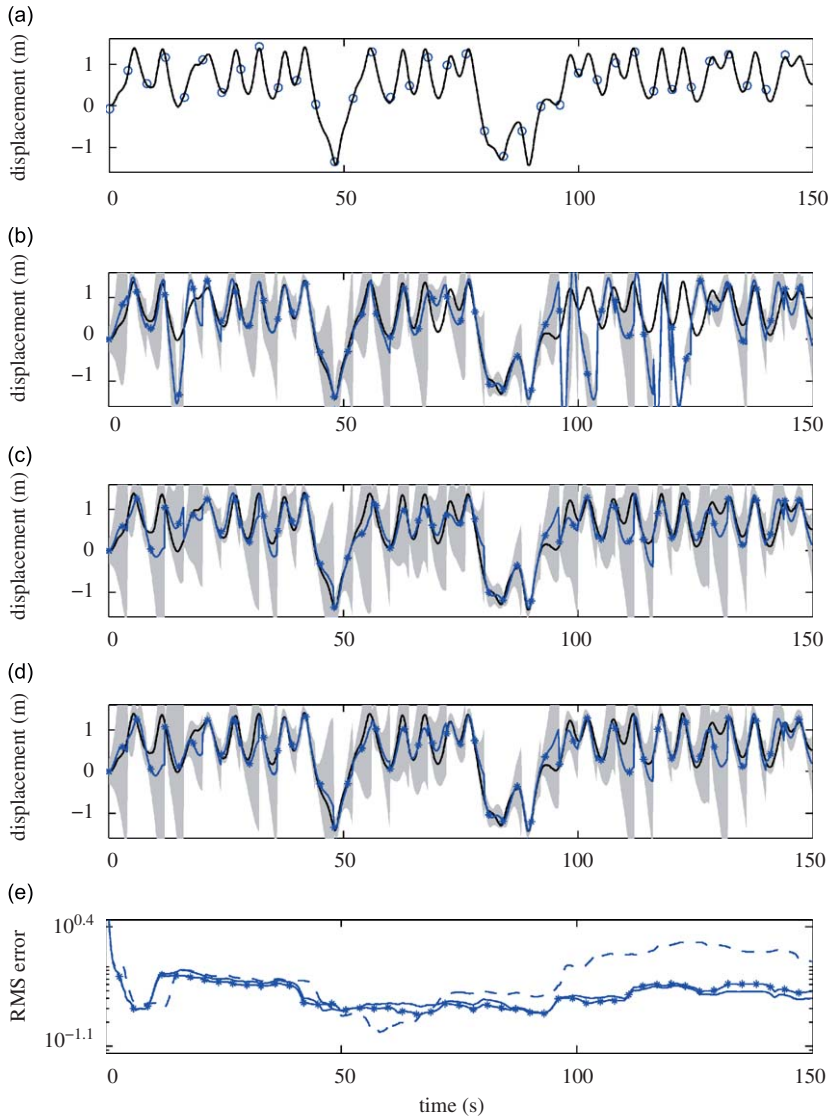

Fig. 15. True, measured and estimated displacement of the Duffing oscillator with sparse measurements for $\mathcal{T} = 0.37$: (a) true (solid line) and measured (circles) displacement; (b) extended Kalman filter estimate (blue line with stars) ± 3 error standard deviations (light blue area); (c) ensemble Kalman filter estimate (blue line with stars) ± 3 error standard deviations (light blue area) with $N = 50$; (d) particle filter estimate (blue line with stars) ± 3 error standard deviations (light blue area) with $N = 50$; and (e) time-averaged normalized root-mean-square estimate errors of the extended Kalman filter (dashed line), ensemble Kalman filter (solid line) and particle filter (solid line with stars). (For interpretation of the references to color in this figure legend, the reader is referred to the web version of this article.)

particle filter provide similarly accurate estimates for both the mean estimate and the associated error standard deviation. The infrequent assimilation of data permits the probability density functions of the state variables to regain their non-Gaussian features over the measurement interval as observed in the transition probability density functions as in Figs. 6 and 7. Such non-Gaussian trends degrade the performance of the extended Kalman filter.

6.4.3. *Effect of modelling uncertainty*

Finally we study the performance of the filters in tracking limit cycle oscillation for the case of higher model uncertainty with $\sigma = 0.5$. The top panels in Figs. 16 and 17 present the true and measured displacement of the oscillator for $\mathcal{T} = 0.3$ and 0.37, respectively. In both cases, the strength of measurement noise is 10 percent of the RMS value of the true displacement. In the same figures, subplots (b), (c) and (d) present the state estimates obtained using the extended Kalman filter, ensemble Kalman filter and particle filter, respectively. All three filters give similar estimates.

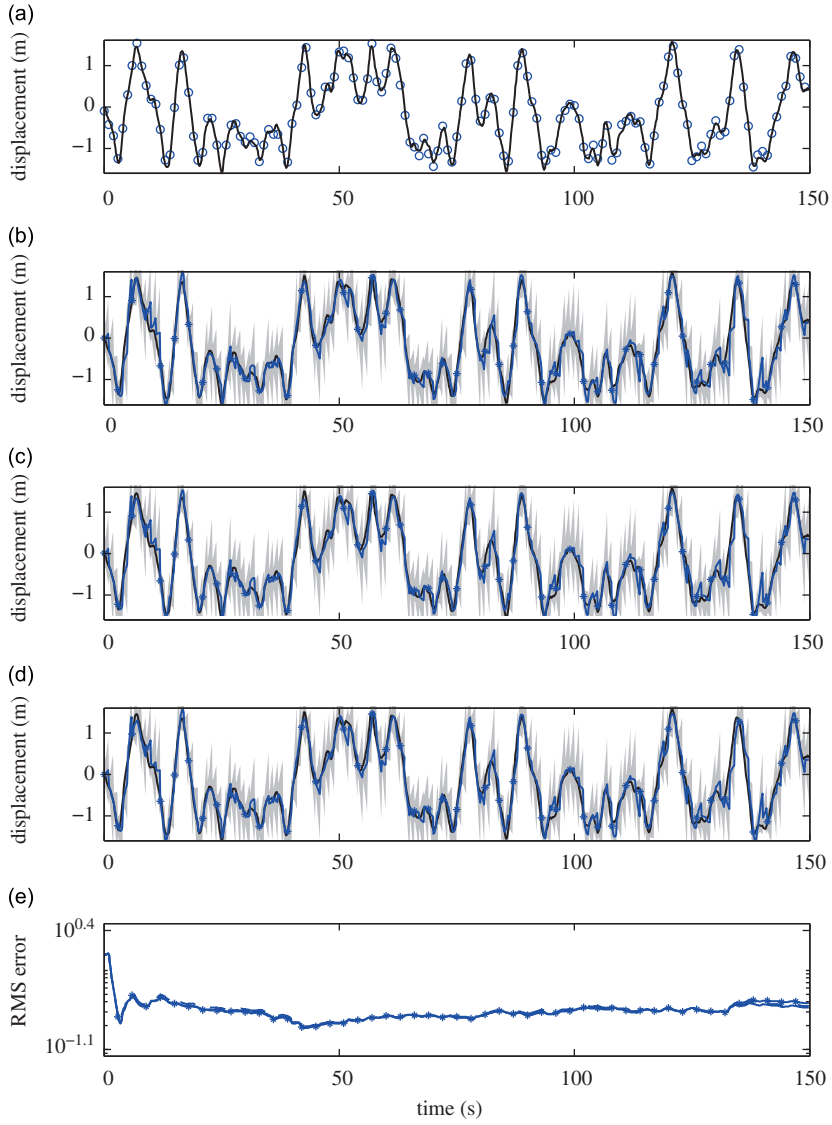

Fig. 16. True, measured and estimated displacement of the Duffing oscillator under greater modelling uncertainty for $\mathcal{T} = 0.3$: (a) true (solid line) and measured (circles) displacement; (b) extended Kalman filter estimate (blue line with stars) ± 3 error standard deviations (light blue area); (c) ensemble Kalman filter estimate (blue line with stars) ± 3 error standard deviations (light blue area) with $N = 50$; (d) particle filter estimate (blue line with stars) ± 3 error standard deviations (light blue area) with $N = 50$; and (e) time-averaged normalized root-mean-square estimate errors of the extended Kalman filter (dashed line), ensemble Kalman filter (solid line) and particle filter (solid line with stars). (For interpretation of the references to color in this figure legend, the reader is referred to the web version of this article.)

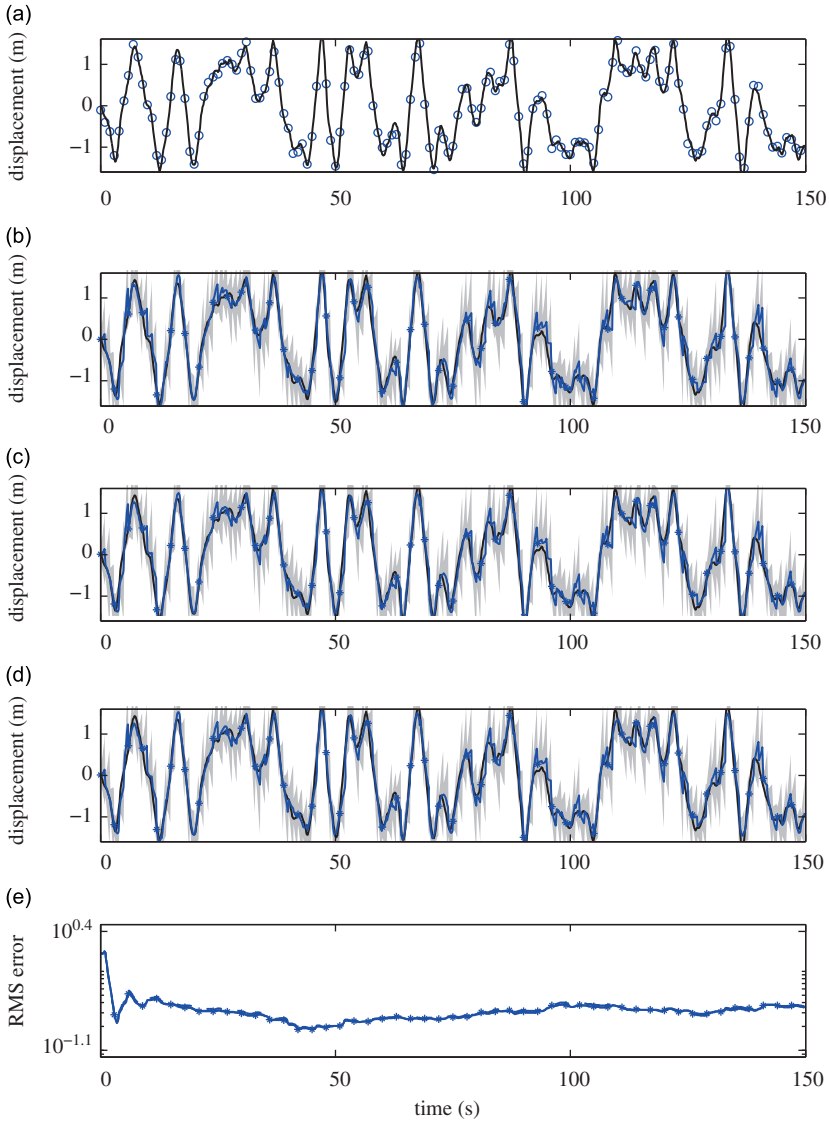

Fig. 17. True, measured and estimated displacement of the Duffing oscillator under greater modelling uncertainty $\mathcal{T} = 0.37$: (a) true (solid line) and measured (circles) displacement; (b) extended Kalman filter estimate (blue line with stars) ± 3 error standard deviations (light blue area); (c) ensemble Kalman filter estimate (blue line with stars) ± 3 error standard deviations (light blue area) with $N = 50$; (d) particle filter estimate (blue line with stars) ± 3 error standard deviations (light blue area) with $N = 50$; and (e) time-averaged normalized root-mean-square estimate errors of the extended Kalman filter (dashed line), ensemble Kalman filter (solid line) and particle filter (solid line with stars). (For interpretation of the references to color in this figure legend, the reader is referred to the web version of this article.)

7. Conclusion

This paper investigates nonlinear filtering techniques, namely the extended Kalman filter, ensemble Kalman filter and particle filter, for the state estimation of noisy limit cycle oscillation. For two cases of limit cycle oscillation of a Duffing system, extensive numerical experiments are conducted to bring out the superiority and limitations of these filters with respect to measurement and modelling errors and sparsity of observational data. For the particular cases studied in this paper, Section Table 1 summarizes the details of the numerical investigations along with the related conclusions. The salient features emerging from this investigation are:

(1) For both limit cycle oscillations, the extended Kalman filter, ensemble Kalman filter and particle filter all perform equally well in tracking the true state of the system for the cases of weak measurement noise and dense observational data. In these cases, the conditioned probability density functions of the system state remains largely Gaussian.

Table 1
Conclusions from the numerical experiments.

Case examined	$\mathcal{T}$	σ	Data acquisition period	Noise to signal variance ratio (percent)	Remarks	Fig.
Low measurement and modelling noise; dense data	0.3	0.01	1 time unit	1	EKF, EnKF and PF perform well	10
Low measurement and modelling noise; dense data	0.37	0.01	1 time unit	1	EKF, EnKF and PF perform well	11
High measurement and low modelling noise; dense data	0.3	0.01	1 time unit	100	EnKF and PF outperform EKF	12
High measurement and low modelling noise; dense data	0.37	0.01	1 time unit	100	EnKF and PF outperform EKF	13
Low measurement and modelling noise, sparse data	0.3	0.01	8 time units	1	EnKF and PF outperform EKF	14
Low measurement and modelling noise, sparse data	0.37	0.01	8 time units	1	EnKF and PF outperform EKF	15
Low measurement and high modelling noise; dense data	0.3	0.05	1 time unit	1	EKF, EnKF and PF perform well	16
Low measurement and high modelling noise; dense data	0.37	0.05	1 time unit	1	EKF, EnKF and PF perform well	17

An ensemble size of $N = 50$ is used in all experiments for the extended Kalman filter (EKF), ensemble Kalman filter (EnKF) and particle filter (PF).

(2) The performance of the ensemble Kalman filter and particle filter is superior to that of the extended Kalman filter when the measurement noise increases. This can be explained from the fact that an increase in the strength of Gaussian measurement noise translates to a conditional probability density functions featuring stronger non-Gaussian traits. Being non-Gaussian filters, the ensemble Kalman filter and particle filter provide the best estimates.
(3) The increase in data sparsity has a detrimental effect on the state estimates of the extended Kalman filter. The ensemble Kalman filter and particle filter both perform reasonably well in the absence of dense measurement data.
(4) Whenever the displacement of the oscillator approaches the unstable fixed point ($u = 0$), the error covariance provided by the filters increases. This is due to the unstable dynamics exhibited by the system in the proximity of zero displacement.

Acknowledgments

The first author acknowledges the support of the Natural Sciences and Engineering Research Council of Canada through the award of a Canada Graduate Scholarship. The second author acknowledges the support of a Discovery Grant from Natural Sciences and Engineering Research Council of Canada and the Canada Research Chair Program. The third author acknowledges the support of the UK Engineering and Physical Sciences Research Council (EPSRC) through the award of an Advanced Research Fellowship and the Royal Society of London for the award of a visiting fellowship at Carleton University, Canada. The computing infrastructure is supported by the Canada Foundation for Innovation (CFI) and the Ontario Innovation Trust (OIT). The authors would like to thank two anonymous reviewers for their comments which improved the manuscript.

References

[1] S.H. Strogatz, *Nonlinear Dynamics and Chaos: With Applications to Physics, Biology, Chemistry, and Engineering*, Addison-Wesley, Reading, MA, 2000.
[2] M.P. Païdoussis, *Fluid–Structure Interactions: Slender Structures and Axial Flow*, second ed., Academic Press, San Diego, California, 1998.
[3] J.M.T. Thompson, H.B. Stewart, *Nonlinear Dynamics and Chaos: Geometrical Methods for Engineers and Scientists*, Wiley, New York, 1986.
[4] F.C. Moon, *Chaotic Vibrations: An Introduction for Applied Scientists and Engineers*, Wiley, New York, 1987.
[5] G.A. Vio, J.E. Cooper, Limit cycle oscillation prediction for aeroelastic systems with discrete bilinear stiffness, *International Journal of Applied Mathematics and Mechanics* 3 (2005) 100–119.
[6] D. Poirel, S.J. Price, Bifurcation characteristics of a two-dimensional structurally non-linear airfoil in turbulent flow, *Journal of Nonlinear Dynamics* 48 (4) (2007) 423–435.
[7] G. Evensen, *Data Assimilation: The Ensemble Kalman Filter*, Springer, Berlin, 2006.
[8] J. Kaipio, E. Somersalo, *Statistical and Computational Inverse Problems*, Springer, New York, 2005.
[9] A.F. Bennett, *Inverse Modeling of the Ocean and the Atmosphere*, Cambridge University Press, Cambridge, UK, 2002.
[10] R.E. Kalman, A new approach to linear filtering and prediction problems, *Journal of Basic Engineering* 82 (1960) 35–45.
[11] R.E. Kalman, R.C. Bucy, New results in linear filtering and prediction theory, *Journal of Basic Engineering* 83 (1961) 95–108.
[12] R.N. Miller, M. Ghill, F. Gauthiez, Advanced data assimilation in strongly nonlinear dynamical systems, *Journal of the Atmospheric Sciences* 51 (8) (1994) 1037–1056.
[13] A.H. Jazwinski, *Stochastic Processes and Filtering Theory*, Academic Press, San Diego, California, 1970.
[14] G. Evensen, Using the extended Kalman filter with a multilayer quasi-geostrophic ocean model, *Journal of Geophysical Research—Oceans* 97 (C11) (1992) 17905–17924.
[15] P. Gauthier, P. Courtier, P. Moll, Assimilation of simulated wind lidar data with a Kalman filter, *Monthly Weather Review* 121 (6) (1993) 1803–1820.
[16] J.K. Uhlmann, Dynamic Map Building and Localization: New Theoretical Foundations, Ph.D. Thesis, University of Oxford, Oxford, UK, 1995.
[17] S.J. Julier, J.K. Uhlmann, A new extension of the Kalman filter to nonlinear systems, *Proceedings of AeroSense: The 11th International Symposium on Aerospace/Defense Sensing, Simulation and Controls, Multi Sensor Fusion, Tracking and Resource Management*, Orlando, Florida, USA, 1997.
[18] A. Sitz, U. Schwarz, J. Kurths, H.U. Voss, Estimation of parameters and unobserved components for nonlinear systems from noisy time series, *Physical Review E* 66 (2002) 016210.
[19] S. Mariani, A. Ghisi, Unscented Kalman filtering for nonlinear structural dynamics, *Nonlinear Dynamics* 49 (2007) 131–150.
[20] E.A. Wan, R. van der Merwe, *Kalman Filtering and Neural Networks, Chapter 7: The Unscented Kalman Filter*, Wiley, New York, 2001.
[21] G. Burgers, P.J. van Leeuwen, G.A. Evensen, Analysis scheme in the ensemble Kalman filter, *Monthly Weather Review* 126 (6) (1998) 1719–1724.

[22] P.J. van Leeuwen, Comment on data assimilation using an ensemble Kalman filter technique, *Monthly Weather Review* 127 (6) (1999) 1374–1377.
[23] J.D. Annan, Parameter estimation using chaotic time series, *TELLUS Series A—Dynamic Meteorology and Oceanography* 57 (5) (2005) 709–714.
[24] R. Ghanem, G. Ferro, Health monitoring for strongly non-linear systems using the ensemble Kalman filter, *Structural Control and Health Monitoring* 13 (1) (2006) 245–259.
[25] G.A. Kivman, Sequential parameter estimation for stochastic systems, *Nonlinear Processes in Geophysics* 10 (3) (2003) 253–259.
[26] R.N. Miller, E.F. Carter, S.T. Blue, Data assimilation into nonlinear stochastic models, *Tellus Series A—Dynamic Meteorology and Oceanography* 51 (2) (1999) 167–194.
[27] G. Evensen, Sequential data assimilation with a nonlinear quasi-geostrophic model using Monte Carlo methods to forecast error statistics, *Journal of Geophysical Research* 99 (C5) (1994) 10143–10162.
[28] J.L. Anderson, S.L. Anderson, A Monte Carlo implementation of the nonlinear filtering problem to produce ensemble assimilations and forecasts, *Monthly Weather Review* 127 (12) (1999) 2741–2758.
[29] T. Bengtsson, C. Snyder, D. Nychka, Toward a nonlinear ensemble filter for high-dimensional systems, *Journal of Geophysical Research—Atmospheres* 108 (24) (2003) 8775.
[30] J. Mandel, J.D. Beezley, Predictor–corrector and morphing ensemble filters for the assimilation of sparse data into high-dimensional nonlinear systems, *Proceedings of the IOAS-AOLS*, *11th Symposium on Integrated Observing and Assimilation Systems for the Atmosphere*, *Oceans*, *and Land Surface*, San Antonio, Texas, USA, 2007, p. 4.12.
[31] B. Ristic, S. Arulampalam, N. Gordon, *Beyond the Kalman Filter: Particle Filters for Tracking Applications*, Artech House, Boston, 2004.
[32] D.T. Pham, Stochastic methods for sequential data assimilation in strongly nonlinear systems, *Monthly Weather Review* 129 (5) (2001) 1194–1207.
[33] P.J. van Leeuwen, A variance-minimizing filter for large-scale applications, *Monthly Weather Review* 131 (9) (1998) 2071–2084.
[34] S. Kim, G.L. Eyink, J.M. Restrepo, F.J. Alexander, G. Johnson, Ensemble filtering for nonlinear dynamics, *Monthly Weather Review* 131 (11) (2003) 2586–2594.
[35] A. Doucet, N. de Freitas, N. Gordon (Eds.), *Sequential Monte Carlo Methods in Practice*, Springer, New York, 2001.
[36] C.S. Manohar, D. Roy, Monte Carlo filters for identification of nonlinear structural dynamical systems, *Sadhana—Academy Proceedings in Engineering Sciences* 31 (Part 4) (2006) 399–427.
[37] V. Namdeo, C.S. Manohar, Nonlinear structural dynamical system identification using adaptive particle filters, *Journal of Sound and Vibration* 306 (2007) 524–563.
[38] S.J. Ghosh, C.S. Manohar, D. Roy, A sequential importance sampling filter with a new proposal distribution for state and parameter estimation of nonlinear dynamical systems, *Proceedings of the Royal Society of London: Series A* 464 (2007) 25–47.
[39] H. Tanizaki, *Nonlinear Filters: Estimation and Applications*, second ed., Springer, Berlin, 1996.
[40] N.J. Gordon, D.J. Salmond, A.F.M. Smith, Novel approach to nonlinear non-Gaussian Bayesian state estimation, *IEE Proceedings—F Radar And Signal Processing* 140 (2) (1993) 107–113.
[41] J. Ching, J.L. Beck, K.A. Porter, Bayesian state and parameter estimation of uncertain dynamical systems, *Probabilistic Engineering Mechanics* 21 (2006) 81–96.
[42] M. Khalil, A. Sarkar, S. Adhikari, Nonlinear filters for chaotic oscillatory systems, *Journal of Nonlinear Dynamics* 55 (1–2) (2009) 113–137.
[43] Y.K. Lin, *Probabilistic Theory of Structural Dynamics*, McGraw-Hill, New York, 1967.
[44] Y.K. Lin, G.Q. Cai, *Probabilistic Structural Dynamics*, McGraw-Hill, New York, 2004.
[45] C.W. Gardiner, *Handbook of Stochastic Methods for Physics, Chemistry and the Natural Sciences*, third ed., Springer, Berlin, 1985.
[46] S. Haykin (Ed.), *Kalman Filtering and Neural Networks*, Wiley, New York, 2001.
[47] C.K. Chui, G. Chen, *Kalman Filtering with Real-time Applications*, third ed., Springer, Berlin, 1999.
[48] J.S. Whitaker, T.M. Hamill, Ensemble data assimilation without perturbed observations, *Monthly Weather Review* 130 (7) (2002) 1913–1924.
[49] G. Evensen, The ensemble Kalman filter: theoretical formulation and practical implementation, *Ocean Dynamics* 53 (4) (2003) 343–367.
[50] M. Mckay, R. Beckman, W. Conover, A comparison of three methods for selecting values of input variables in the analysis of output from a computer code, *Technometrics* 21 (1979) 239245.
[51] A. Olsson, G. Sandberg, Latin hypercube sampling for stochastic finite element analysis, *Journal of Engineering Mechanics* 128 (2002) 121125.
[52] J. Guckenheimer, P. Holmes, *Nonlinear Oscillations, Dynamical Systems, and Bifurcation of Vector Field*, Springer, New York, 1983.
[53] S. Lynch, *Dynamical Systems with Applications Using MATLAB*, Birkhäuser, Boston, 2004.
[54] G. Maruyama, Continuous Markov processes and stochastic equations, *Rendiconti del Circolo Matematico di Palermo* 4 (1955) 48–90.
[55] Message Passing Interface 〈http://www.mpi-forum.org/〉.